Applied Catalysis B: Environmental 256 (2019) 117792

Contents lists available at ScienceDirect

Applied Catalysis B: Environmental

journal homepage: www.elsevier.com/locate/apcatb

Copper and cobalt nanoparticles doped nitrogen-containing carbon frameworks derived from CuO-encapsulated ZIF-67 as high-efficiency catalyst for hydrogenation of 4-nitrophenol

Changshun Chu, Shun Rao, Zhanfang Ma*, Hongliang Han*

Department of Chemistry, Capital Normal University, Beijing, 100048, China

ARTICLE INFO

Keywords:
4-Nitrophonel
CuO
ZIF-67
Pyrolysis
Hydrogenation

ABSTRACT

4-Nitrophenol (4-NP) in industrial and agricultural wastewater has serious toxic effects on human beings and animals, it is urgent and meaningful to deal with this pollutant. At present, catalysts containing noble metals have been used to catalyze hydrogenation of 4-NP, but noble metals are inevitably costly and limited in supplies. Thus, we presented a facile method to prepare copper and cobalt nanoparticles doped nitrogen-containing carbon frameworks (Cu/Co@NCF) derived from CuO-encapsulated ZIF-67 to replace noble-metal catalysts to eliminate 4-NP. In this work, ZIF-67 was a sacrificial template, the derivative of ZIF-67 acted as not only supported material but also a synergistic catalyst. Due to the high specific surface area and porous ZIF-67, the fusion of copper and cobalt at high temperature was suppressed, resulting in the well distribution of copper and cobalt nanoparticles in the N-containing carbon frameworks during pyrolysis thus enhancing the catalytic performance of the composite. The composite was used as catalyst for hydrogenation of 4-NP, which exhibited perfect catalytic activity. The pseudo-first-order reaction kinetic constant reached 4.159 min^{*}, the specific activity of Cu/Co@NCF-15 was 4 $\mu\text{mol}\cdot\text{mg}^{-1}\cdot\text{min}^{*}$, which was much higher than a number of noble-metal catalysts, making it a potential catalyst for reduction of 4-NP in industrialization.

1. Introduction

4-Nitrophonel (4-NP) is a nitro-compound which can be used as the intermediate of dyes, medicines and pesticides [1–3]. Although 4-NP is a chemical material closely related to chemical production, it is also identified as a kind of priority organic pollutant by the USA EPA [4]. Besides, it has a high polarity and therefore has high solubility in water and exhibits high bioavailability [5]. It is urgent and meaningful to treat 4-NP in industrial and agricultural wastewater due to the toxic effects of 4-NP on the nervous system, viscera and blood of human beings and animals [6]. So far, various approaches have been developed to deal with this organic contaminant, such as adsorption [7,8], Fenton degradation [3,9], photocatalytic degradation [10,11], catalytic degradation (including reductive and oxidative degradation) [12–14], etc. Among these approaches, catalytic reductive degradation is a method of reducing 4-NP to 4-aminophenol (4-AP), which is also a kind of widely used industrial material [15].

Benefited from the irreplaceable physicochemical properties of noble metals (Pt, Au, Ag, etc.), they have been widely used in catalysis [16], optoelectronics [17], fuel cell [18], sensor in recent years [19,20]. Especially, noble metal nanomaterials have been extensively used in the hydrogenation reduction of 4-NP in the participation of sodium borohydride ($NaBH_4$) as catalysts in the industrial and agricultural wastewater treatment [21–25]. Nevertheless, because of the high price of noble metals and their limited supplies, there is a desired requirement to use non-noble metals as a substitute for these noble metals. Among the non-noble metals, copper nanoparticles (Cu NPs) have attracted considerable attention due to their cost effectiveness, stable nature and the fact that Cu NPs can be used as a substitute for noble metals to catalyze hydrogenation of nitroaromatic compounds under mild conditions, achieving a great conversion rate at ambient temperature [26,27]. However, naked metal nanoparticles without protection or support suffer from a problem, on account of the high surface energy of metal nanoparticles, they will gradually aggregate and precipitate in aqueous media, reducing their catalytic activity, stability and reusability [26,28]. To overcome the shortcoming, support materials such as SiO_2, carbon materials and hydrogels have been used to prevent the adverse effects of aggregation and precipitation [29–31]. These support materials are inert and are just employed to offer enough attachment sites and space to ensure the anchoring and well dispersion of metal

* Corresponding authors.
E-mail addresses: mazhanfang@cnu.edu.cn (Z. Ma), hanhongliang@cnu.edu.cn (H. Han).

https://doi.org/10.1016/j.apcatb.2019.117792
Received 26 January 2019; Received in revised form 12 May 2019; Accepted 28 May 2019
Available online 29 May 2019
0926-3373/

nanoparticles thus maintaining their intrinsic activity. In addition of enhancing catalytic activity by keeping the activity of metal nanoparticles, imparting superior catalytic ability to the support material is also an effective protocol to magnify the holistic catalytic effect of the metal-based catalysts.

Herein, in order to combine transition metal nanoparticles with catalytically active support materials to promote the catalytic activity of the whole metal-based catalysts, we presented a facile method to prepare Cu NPs and cobalt nanoparticles (Co NPs) doped N-containing carbon frameworks (Cu/Co@NCF). ZIF-67, a kind of MOF with large specific surface area, porous structure and designable frameworks [32–34], was utilized to encapsulate CuO to form the precursor of Cu/Co@NCF. In this composite catalyst, transition metal nanoparticles Cu NPs and Co NPs were anchored in the N-containing carbon frameworks (NCF) which derived from ZIF-67 during pyrolysis, NCF acted as not only support material for Cu NPs and Co NPs but also a synergistic catalyst. Compared with most noble-metal catalysts and transition metal catalysts previously reported, the catalyst we prepared possessed higher catalytic activity for the reduction of 4-NP due to the introduction of Cu NPs as well as the doped Co NPs and N-containing carbon frameworks can promote the reduction of 4-NP, the catalyst had good recycling performance as well.

2. Experimental

2.1. Chemicals

Copper acetate monohydrate ($Cu(CH_3COO)_2{\cdot}H_2O$) and cobalt nitrate hexahydrate ($Co(NO_3)_2{\cdot}6H_2O$) were purchased from Alfa Aesar (Shanghai, China). Polyvinylpyrrolidone (PVP) with a molecular weight of 55,000 and sodium borohydrate ($NaBH_4$) were obtained from Sigma-Aldrich (Beijing, China). Methanol was purchased from Merck KGaA (Beijing, China). 2-Methylimidazole (2-MeIM) was obtained from Acros (Beijing, China). 4-Nitrophenol (4-NP) was purchased from Innochem (Beijing, China). Ethanol was purchased from Fuchen (Tianjin) chemical reagents Co., LTD. The water used in this work was deionized water (resistivity was about 18.2 MΩ cm).

2.2. Preparation of CuO

CuO was prepared according to a previously reported approach [35]. Briefly, 50 ml ethanol solution of copper acetate (0.05 M) was added into a Teflon liner stainless steel autoclave, then put the autoclave into an oven and the reaction was carried out at about 110 °C for 20 h. After 20 h, the autoclave was cooled to ambient temperature naturally. The resulting black powder was centrifuged, then washed three times in ethanol after being washed two times in deionized water, and finally dried under vacuum at ambient temperature for further use.

2.3. Synthesis of PVP-modified CuO (PVP-CuO)

PVP-modified CuO was synthesized as follows, CuO that was prepared above was added into 25 mL methanol under ultrasonic condition until there was no precipitate, then 600 mg PVP was added into the methanol solution of CuO, the obtained solution was kept magnetic stirring for 24 h. After 24 h, the PVP-modified CuO was collected by centrifugation, washed three times in methanol, and then dried under vacuum at room temperature for further application.

2.4. Synthesis of CuO-encapsulated ZIF-67

CuO@ZIF-67 was fabricated by the method of bottle-around-a-ship. Typically, PVP-CuO (5, 10, 15, 20 mg) was dispersed in 25 mL methanol under ultrasonic condition until there was no precipitate, then 291 mg $Co(NO_3)_2{\cdot}6H_2O$ and 200 mg PVP were mixed with the resulting solution under magnetic stirring for 30 min. Subsequently, 328 mg of 2-MeIM was added into 25 mL methanol, the obtained clear solution was slowly injected into the solution of mixture. After 24 h, the final purple product was collected by centrifugation (6000 r/min), washed three times in methanol drastically to remove surfactant and uncoordinated residues, and finally dried at 60 °C under vacuum for 12 h. ZIF-67 without CuO was prepared with the same approach. The obtained CuO@ZIF-67 with different mass of CuO were denoted as CuO@ZIF-67-X (X = 5, 10, 15, 20).

2.5. Synthesis of CuO@ZIF-67 derivatives (Cu/Co@NCF-X)

Cu/Co@NCF-X (X = 5, 10, 15, 20) and Co@NCF were compounded through the pyrolysis of CuO@ZIF-67-X (or ZIF-67) at 800 °C under an argon atmosphere for 2 h with a heating rate of 5 °C min^{-1}. In addition, the composite denoted as Cu/Co/NCF was synthesized by pyrolyzing the mixture of 26 mg $Cu(CH_3COO)_2{\cdot}H_2O$ and 100 mg ZIF-67 through the similar procedure at the same conditions. The pure Cu NPs were synthesized by hydrothermal reaction [36].

2.6. Characterization

The morphology of the samples was observed by using the scanning electron microscope (SEM) of SU-8000 (Hitachi, Japan) and the high resolution transmission electron microscopy (HRTEM) of JEM-2100 F (JEOL, Japan). Energy dispersing X-ray spectroscopy (EDS, Oxford instruments X-Max) was used to investigate the elemental composition of the Cu/Co@NCF. Inductively coupled plasma mass-spectrometry (ICP-MS) was conducted on Agilent 7500Ce (Agilent Technologies, America). X-ray powder diffraction (XRD) was characterized by Bruker D8 ADVANCE (Bruker, Germany). The specific surface area and pore volume analysis were investigated by Brunauer-Emmett-Teller (BET, Quantachrome NOVA 1000e) from the nitrogen adsorption and desorption isotherms at 77 K. X-ray photoelectron spectroscopy (XPS) measurements were carried out by using an ESCALAB 250 (ThermoFisher Scientific, USA). UV/Vis spectra have been investigated on a Shimadzu UV-2550 spectrophotometer with the wavelength range from 260 to 500 nm at room temperature.

2.7. Catalytic hydrogenation reduction of 4-nitrophenol

Catalytic hydrogenation reduction of 4-NP was conducted in a 4 mL quartz cuvette in the presence of excessive $NaBH_4$, the catalytic hydrogenation reduction process was monitored by using a Shimadzu UV-2550 spectrophotometer at room temperature. Typically, 3 mL 0.1 mM 4-NP was injected into the quartz cuvette, then 0.3 ml 0.2 M freshly prepared $NaBH_4$ was added into 4-NP solution, resulting in the color change from light yellow to bright yellow. Subsequently, 5 μL Cu/Co@NCF-X suspension (10 mg/mL) was added to the mixture solution under ultrasonic condition for 10 s, and the catalytic hydrogenation process was monitored by the UV/Vis measurements with the wavelength range from 260 to 500 nm. The catalytic performances of Co@NCF, pure Cu NPs (1.6×10^{-3}mg, the mass of Cu NPs was based on the ICP-MS analysis below), Cu/Co/NC, the mixture of pure Cu NPs and Co@NCF (pCu/Co) were also valued through the similar procedure. To evaluate the reusability of Cu/Co@NCF-15, it was separated and recycled for 5 times.

3. Results and discussion

3.1. Catalyst preparation and characterization

The preparation process of Cu/Co@NCF is as shown in Scheme 1. In a nutshell, the pre-fabricated CuO stabilized by PVP was coated with a ZIF-67 to form CuO@ZIF-67 which possessed the core-shell structure. CuO@ZIF-67 had an open-framework structure in which Co ions coordinated with N atoms in 2-MeIM links to form tetrahedral CoN4

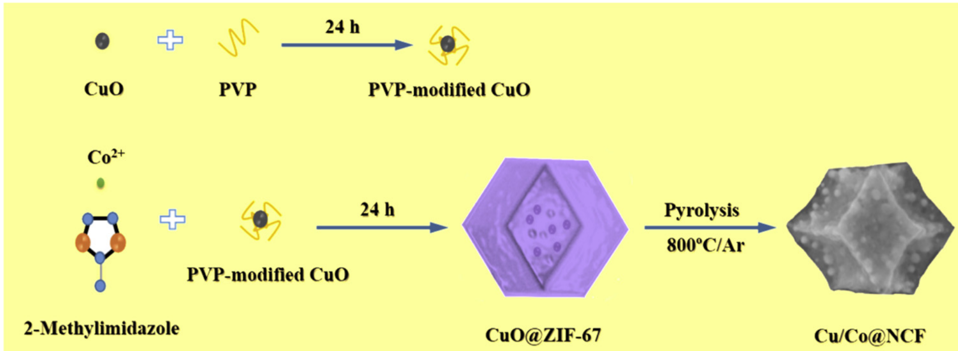

Scheme 1. Illustration of the fabrication of Cu/Co@NCF.

building units thus forming the rhombic dodecahedral morphology [37], then it was pyrolyzed in argon atmosphere at a high temperature to obtain the Cu-based composite. After pyrolysis, Cu NPs and Co NPs can be well distributed in NCF because of the confinement effect of the porous structure of ZIF-67 [38]. In the fabrication process, CuO was the source of copper, ZIF-67 was the source of carbon, nitrogen and cobalt as well as the sacrificial template, the resulting NCF during pyrolysis was the support material. The obtained composite was used as catalyst for hydrogenation of 4-NP in the presence of $NaBH_4$.

As shown in Fig. 1(a–b), the scanning electron microscope (SEM) images clearly showd that the fabricated CuO@ZIF-67 had the same morphology as the pristine ZIF-67 in the formerly reported literatures [39,40], and CuO@ZIF-67 had an average diameter of about 1.2 μm. It can be obviously observed from Fig. 1c that CuO was encased in ZIF-67. The mapping images (Fig. 1d–g) showed the distribution of elements of C, N, Co and Cu, further confirming the successful encapsulation of CuO into ZIF-67.

In order to examine the crystal structure of CuO@ZIF-67, X-ray powder diffraction (XRD) was introduced to analyze the sample. As shown in Fig. 2, the characteristic diffraction peaks in XRD patterns represented pristine ZIF-67 and CuO@ZIF-67, respectively. By comparing the XRD patterns of them, we realized that all the characteristic peaks associated with ZIF-67 all exist in the XRD pattern of CuO@ZIF-67, indicating that CuO encapsulated in ZIF-67 would not damage its crystal structure. From the XRD pattern of CuO@ZIF-67, the characteristic peaks of CuO (Fig. S1) corresponded to the facets (11-1), (111), (20-2), (202), (11-3), (31-1) at 2θ of 35.5°, 38.7°, 48.7°, 58.3°, 61.5°, 66.2° (Jade card no. 48-1548) were clearly identified, which further proved that CuO was indeed encapsulated in ZIF-67 and the structure of ZIF-67 was intact as pristine one.

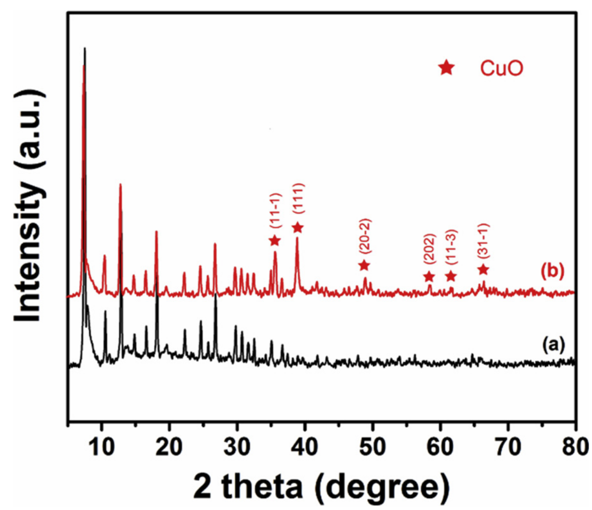

Fig. 2. XRD patterns of (a) pristine ZIF-67 and (b) CuO@ZIF-67.

To observe the morphology of Cu/Co@NCF, SEM and HRTEM were

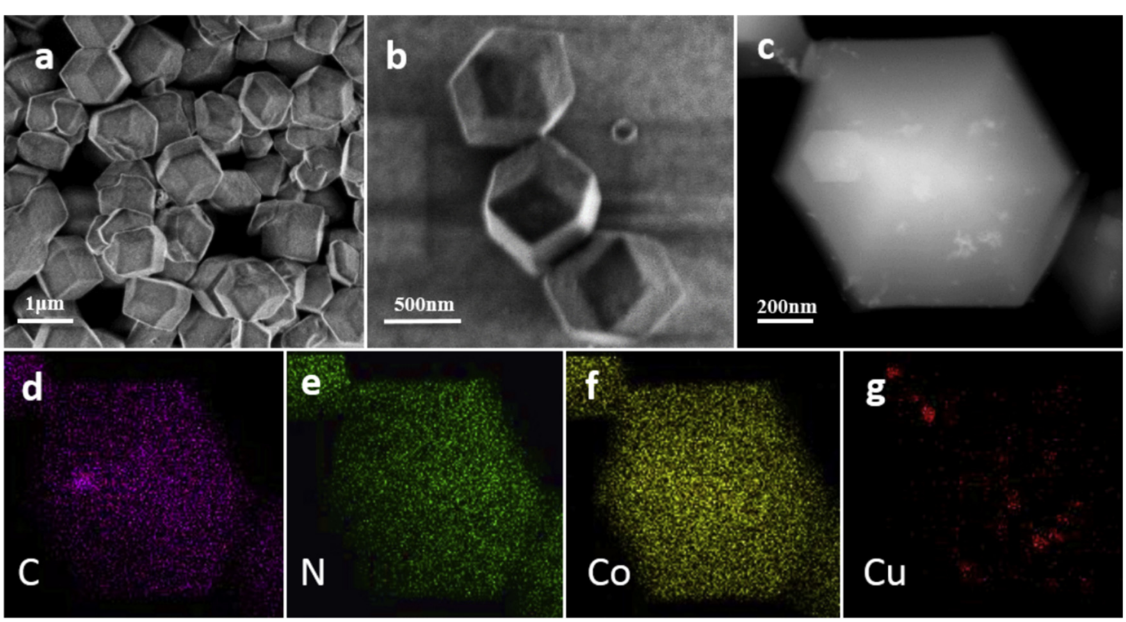

Fig. 1. SEM images of (a–b) CuO@ZIF-67-15, HRTEM image of (c) CuO@ZIF-67-15 and mapping images of the as-prepared (d–g) CuO@ZIF-67-15.

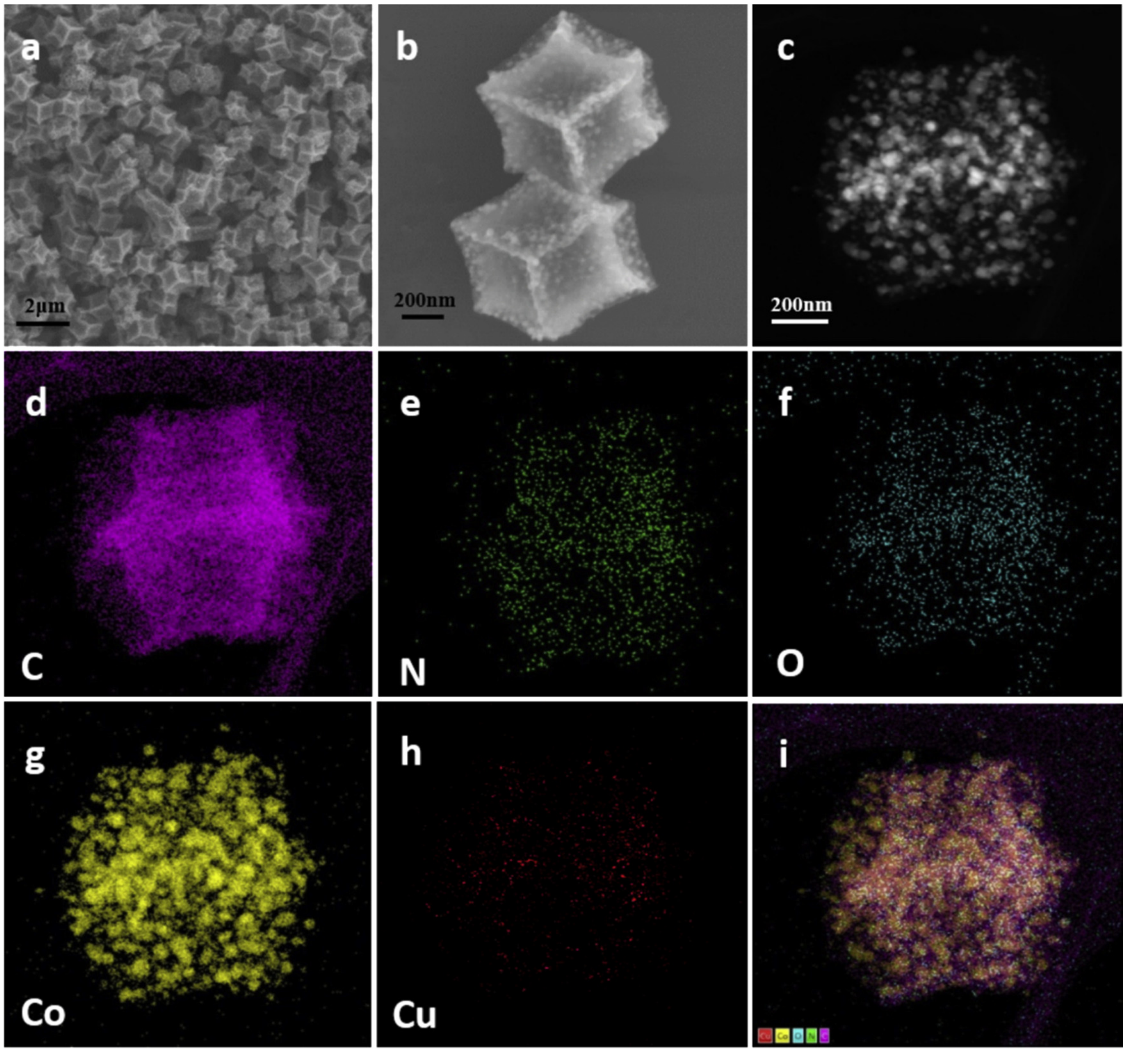

Fig. 3. SEM images of (a–b) Cu/Co@NCF-15, HRTEM image of (c) Cu/Co@NCF-15 and mapping images of the as-prepared (d–i) Cu/Co@NCF-15.

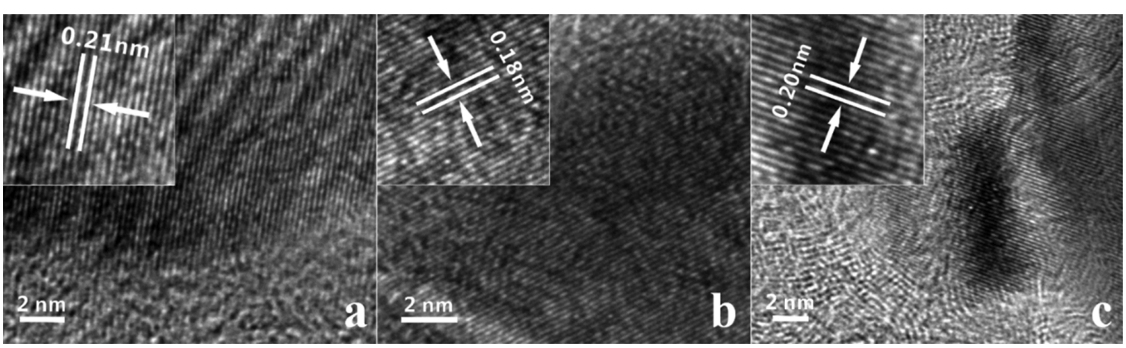

Fig. 4. HRTEM images of (a–b) Cu NPs and (c) Co NPs. (IFFT images were illustrated in each figure, representing the (111), (200) planes of Cu NPs and the (111) plane of Co NPs, respectively).

conducted. The images (Fig. 3a and b and Fig. S2a) showed that the surface of Cu/Co@NCF-15 became rough and inward concave. Due to the loss of a number of organic part during pyrolysis, the framework was shrunk to be about 1 μm. Nevertheless, Cu/Co@NCF-15 still retained the shape of rhombic dodecahedron like ZIF-67. The HRTEM images (Fig. 3c and Fig. S2b) showed that numerous nanoparticles with the sizes about 15–70 nm were embedded into the carbon frameworks. Besides, obvious porous structure can be seen as well, the pores were evenly distributed inside and outside the carbon framework, allowing the reactants efficiently diffusing and transferring to the active site of the catalyst [41]. For comparison, the morphology of Cu/Co/NCF can be seen in Fig. S3, the structure of dodecahedron was destroyed and the copper and cobalt were sintered into much larger NPs when compared with the size of NPs in Cu/Co@NCF-15, illustrating that encapsulation of CuO into porous ZIF-67 was an effective method to inhibit the self-agglomeration of Cu and Co NPs as well as maintain the complete structure of carbon framework during pyrolysis. The specific surface area and porosity of Cu/Co@NCF-15 was further confirmed by N_2 adsorption-desorption isotherms (Fig. S4), it can be seen that the sample owns type-IV isotherms with sharp N_2 uptakes and obvious hysteresis

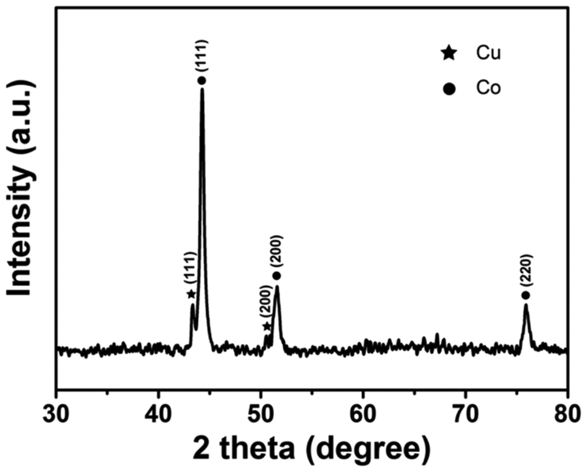

Fig. 5. XRD pattern of Cu/Co@NCF-15.

loops, demonstrating that the sample had microporous and porous structures [42]. The mean pore size is about 6.4 nm which can be obtained from BET test. From the energy dispersive X-ray spectroscopy (EDS, Fig. S5), we can know that the content of C, N, O, Co and Cu are 51.9%, 2.0%, 8.5%, 32.2% and 5.4%, respectively. It should be noted the ICP-MS analysis manifested that the content of Cu element was 3.5 wt%. The mapping images (Fig. 3d-i) showed the distribution of various elements in Cu/Co@NCF-15. In particular, comparing the mapping images of CuO@ZIF-67 and Cu/Co@NCF-15, it can be found that Cu were uniformly dispersed throughout the carbon framework rather than aggregation. Fig. 4 illustrated the HRTEM images of Cu NPs and Co NPs, the lattice spacings of 0.21 and 0.18 nm (Fig. 4a and b) were attributed to the (111) and (200) planes of Cu NPs, 0.20 nm was attributed to the (111) plane of Co NPs, manifesting that Cu NPs and Co NPs were synthesized during pyrolysis.

To analyze the existence status of the copper and cobalt elements in the obtained Cu/Co@NCF-15, XRD was employed to characterize their crystal structures. It can be observed from Fig. 5 that two characteristic peaks at 2θ of 43.3° and 50.4° corresponded to the (111) and (200) facets of copper (Jade card no. 04-0836), respectively. The characteristic peaks at 2θ of 44.2°, 51.6° and 75.9° were related to the (111), (200) and (220) facets of cobalt (Jade card no. 15-0806). These results proved that CuO and cobalt ions were reduced to simple substance during pyrolysis.

X-ray photoelectron spectroscopy (XPS) was further carried out to investigate the elemental species present in Cu/Co@NCF-15. The characteristic survey spectrum shown in Fig. 6a demonstrated that Cu/Co@NCF-15 was formed from C, N, O, Co and Cu, it further proved that Cu NPs was successfully doped into Cu/Co@NCF. The high resolution N 1s XPS spectrum was shown in Fig. 6b, the four peaks at 398.3 eV, 399.0 eV, 400.5 eV and 401.1 eV showed the existence of pyridinic-N, Co-N, pyrrolic-N and graphitic-N [38,43]. As shown in Fig. 6c, compared to Co@NCF, the content of N in Cu/Co@NCF-15 increased, indicating that the introduction of Cu can reduce the loss of N during pyrolysis. The high resolution Cu $2p_{3/2}$ XPS spectrum was shown in Fig. 6d, two peaks at 932.7 and 934.8 eV were related to Cu (0) or Cu (I), and Cu (II) [44,45]. The high resolution spectrum of Co $2p_{3/2}$ (Fig. 6e) showed characteristic peaks at 778.4 eV, 780.1 eV, and 781.6 eV, corresponding to Co, CoOx or CoCxNy, and Co-N, respectively [46–48].

3.2. Catalytic reduction of 4-NP

Catalytic reduction of 4-NP to 4-AP was carried out in aqueous solution in the presence of excessive NaBH4 at room temperature. Metal particles in supported materials can accelerate the transfer of electrons from borohydride to electron acceptor 4-NP, leading to the hydrogenation reduction of 4-NP to 4-AP [27]. Besides, NCF can also promote the reduction of 4-NP in that the doped N atoms that contain abundant valence electrons can generally heighten the π-electron density in the carbon frameworks to improve the electrical properties and the surface reactivity of NCF [43]. As is known, the color of 4-NP will change from light yellow to bright yellow after the addition of $NaBH_4$ due to the generation of 4-nitrophenolate when pH of the solution changes from neutral to alkaline. Accordingly, the UV/Vis absorption peak of 4-NP shifted from 317 nm to 400 nm for 4-nitrophenolate as was shown in Fig. 7a. When there was no catalyst added into the mixture solution, the absorption peak at 400 nm did not change significantly within one hour (Fig. 7b), suggesting that the addition of $NaBH_4$ cannot reduce 4-NP in the absence of catalyst in a period of time. After Cu/Co@NCF-X was added, the peak at 400 nm decreased rapidly, while a new absorption peak corresponding to 4-AP appeared at 300 nm (Fig. 7c). When the catalytic process was over, the color of the mixture solution became colorless. By monitoring the intensity of the absorption peak at 400 nm, it can be found that when the amount of catalyst (Cu/Co@NCF-15) was only 0.05 mg, the absorption peak disappeared within 1.5 min (the catalytic results of Co@NCF, Cu/Co@NCF-5, Cu/Co@NCF-10 and Cu/Co@NCF-20 can be seen in Fig. S6), substantiating that the catalyst we prepared had high catalytic efficiency in catalytic reduction of 4-NP. Through the kinetic analysis, the conversion of 4-NP can be obtained by calculating the relationship between C_t/C_0 (C_t and C_0 represented the concentration of 4-NP at time t and the initial concentration of 4-NP) and time at 400 nm, as shown in Fig. 7d. Meanwhile, the UV/Vis absorbance spectra of 4-NP catalyzed by pure Cu NPs, pCu/Co and Cu/Co/NCF were also shown in Fig. 8. 4-NP was only reduced by approximately 1.8% in 12 min in the presence of Cu NPs (Fig. 8a), while 4-NP was completely reduced in 4 and 5 min in the presence of pCu/Co and Cu/Co/NCF (Fig. 8b and c). Since the amount of $NaBH_4$ was much higher than 4-NP, it can be considered that the amount of $NaBH_4$ did not change during the catalytic reaction, thus the catalytic reduction of 4-NP was a pseudo-first-order reaction and the kinetic equation was $\ln(C_t/C_0) = -kt$ (k represents the apparent pseudo-first-order rate constant, min^{-1}). The constant k value of Cu/Co@NCF-15 was 4.159 min^{-1}, which was almost three times of that of Co@NCF (1.398 min^{-1}). Besides, the rate constant k values of Cu/Co@NCF-5, Cu/Co@NCF-10, Cu/Co@NCF-20, pCu/Co and Cu/Co/NCF were 2.221, 2.791, 3.695, 1.422, and 1.058 min-1, respectively. By comparing the rate constant k values of Cu/Co@NCF-15 and Cu/Co/NCF, it can be inferred that the aggregation of metal NPs and the destruction of the carbon framework would lead to a decrease of catalytic performance of the catalyst. What is more, Cu/Co@NCF-15 had better catalytic performance than pure Cu NPs and pCu/Co, manifesting that Cu NPs anchored in the derivative of ZIF-67 can effectively synergistically catalyze reduction of 4-NP. The above results demonstrated that Cu/Co@NCF-15 own the best catalytic effect toward 4-NP, thus it was meaningful and important to introduce Cu NPs into Co@NCF and consider the effect of copper content on the catalyst as well as the method of introduction. The catalytic performance of Cu/Co@NCF-15 was also tested after it was placed in the air for 7 (Cu/Co@NCF-15-7) and 21 days (Cu/Co@NCF-15-21) at room temperature (Fig. S7), the k values of Cu/Co@NCF-15-7 and Cu/Co@NCF-15-21 were 3.951 and 3.103 min-1. 4-NP can be reduced completely in 2 min when Cu/Co@NCF-15-21 was used, which proved that catalyst still had excellent catalytic performance after 21 days. In order to further evaluate the catalytic activity of Cu/Co@NCF-15, noble-metal catalysts and non-metal catalysts were introduced for comparison. It can be seen from Table S1 that Cu/Co@NCF-15 has a highest specific activity of 4 μmol· mg^{-1}· min^{-1} and highest turnover frequency (TOF) of 7.26 min^{-1}, indicating that Cu/Co@NCF-15 was more effective and excellent for the reduction of 4-NP. The possible mechanism of copper enhanced catalytic performance is described below. Copper, like other noble metals, has good electrical conductivity and can rapidly transfer electrons of electron donors adsorbed on its surface to the

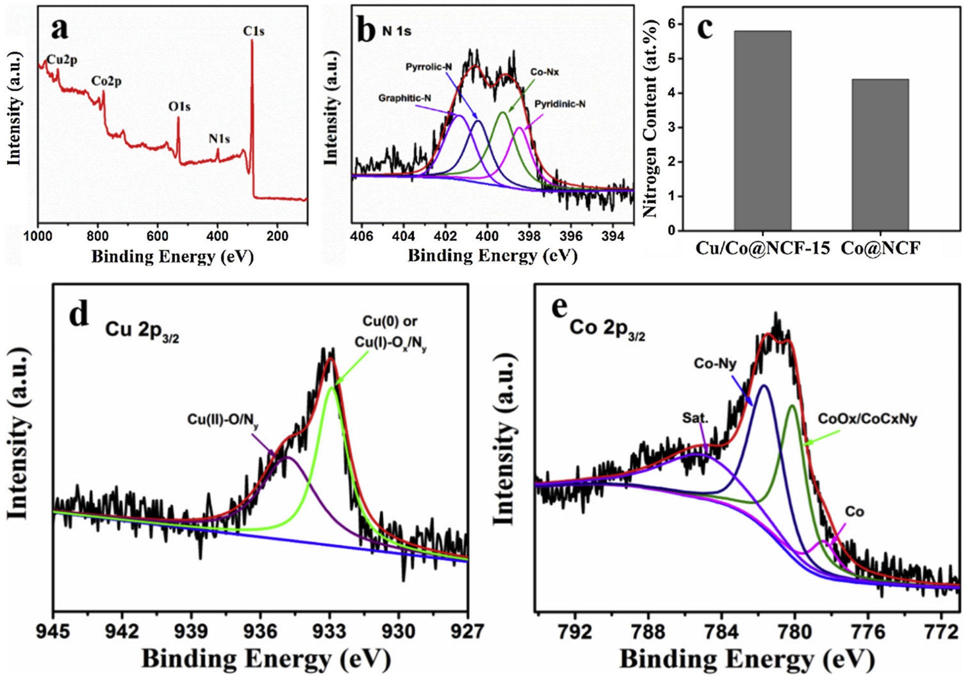

Fig. 6. XPS spectra of the (a) Cu/Co@NCF-15, the high-resolution XPS spectrums of (b) N 1S, (d) Cu $2p_{3/2}$ and (e) Co $2p_{3/2}$, and (c) the N content of Cu/Co@NCF-15 and Co@NCF.

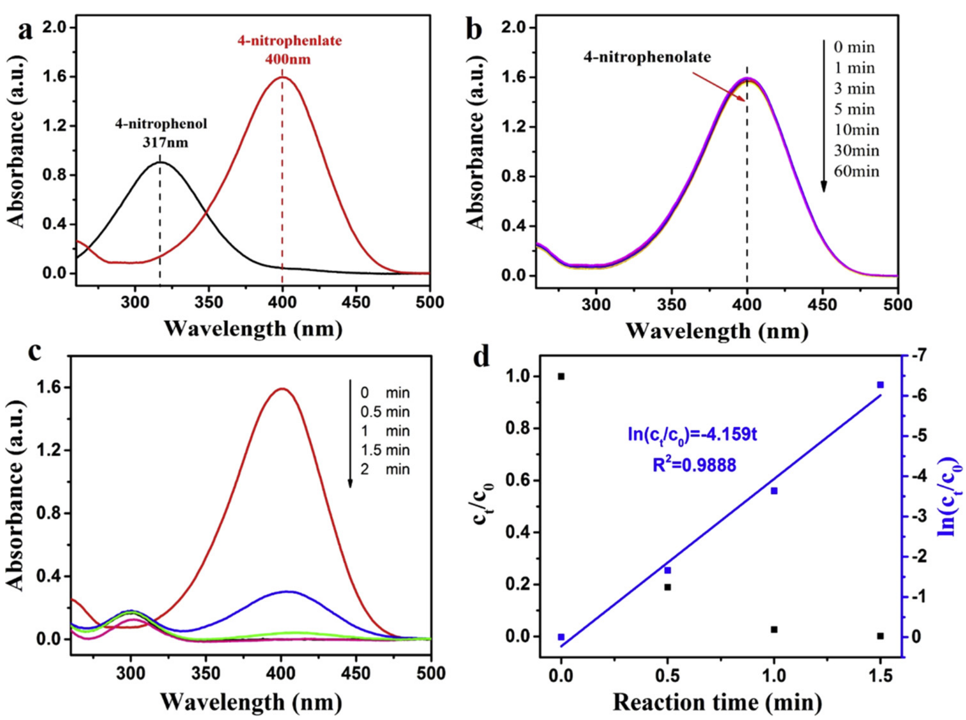

Fig. 7. UV/Vis absorption spectra of (a) 4-NP before and after addition of excessive $NaBH_4$ solution, time-dependent UV/Vis absorption spectrum of 4-NP in the presence of $NaBH_4$ solution (b) without catalyst and (c) with Cu/Co@NCF-15 and (d) plots of C_t/C_0 and $\ln(C_t/C_0)$ against the reaction time for Cu/Co@NCF-15.

acceptors, leading to the acceleration of reactions [49–51]. According to the previously reported catalytic processes of Ag and Au catalyst toward 4-NP [52,53], the possible reduction process is depicted in Scheme 2. $NaBH_4$ was adsorbed and desorbed synchronously on the surface of Cu NPs, and a copper hydride was also formed at the same time. Subsequently, hydrogen and electrons transferred to the nitro group of 4-NP, which was converted into 4-AP after hydrogenation. 4-AP was then desorbed from the Cu NPs and took part in catalytic reaction again.

Whether the catalyst can be reused is an important factor for practical application evaluation. Therefore, to assess the reusability and stability of the catalyst, Cu/Co@NCF-15 was reused for five times by magnetic separation (Fig. S8), and the conversion rate of 4-NP is still almost 94% after five successful cycles (Fig. 9). It proves that Cu/Co@NCF-15 has good stability and reusability with the potential use in industrialization.

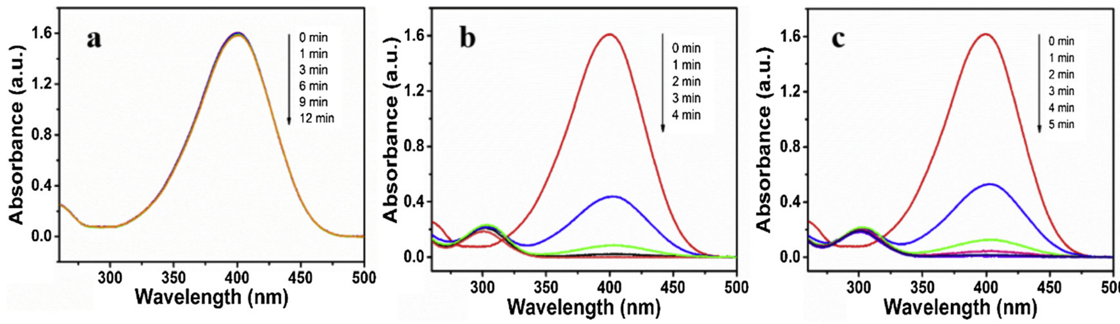

Fig. 8. UV/Vis absorption spectra of 4-NP during the reduction process catalyzed by (a) Cu NPs, (b) pCu/Co and (C) Cu/Co/NCF in the presence of excessive $NaBH_4$.

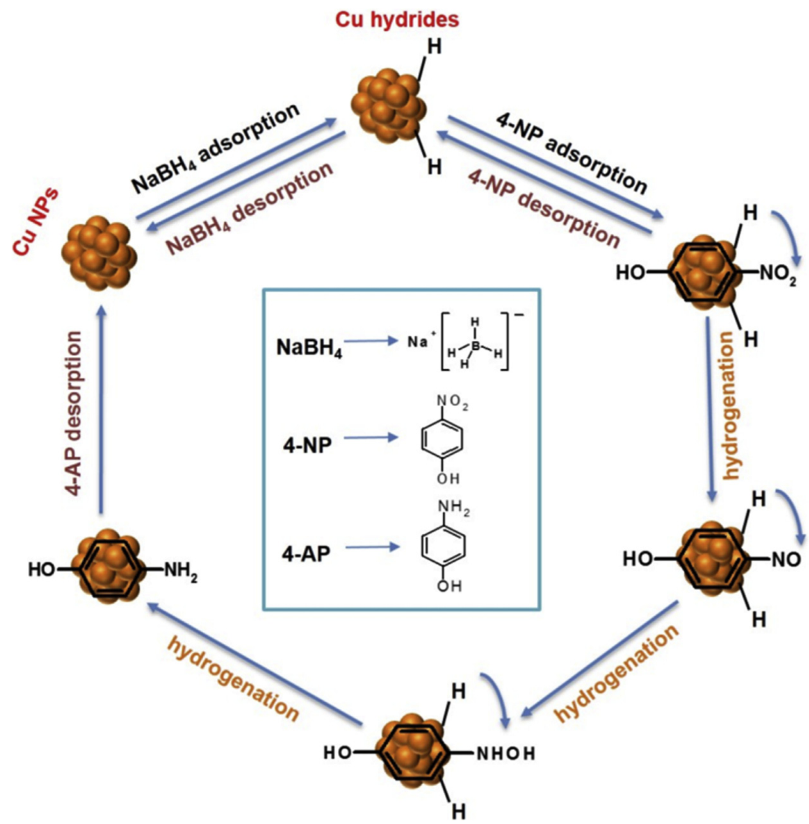

Scheme 2. The possible reduction process of 4-NP on the surface of Cu NPs.

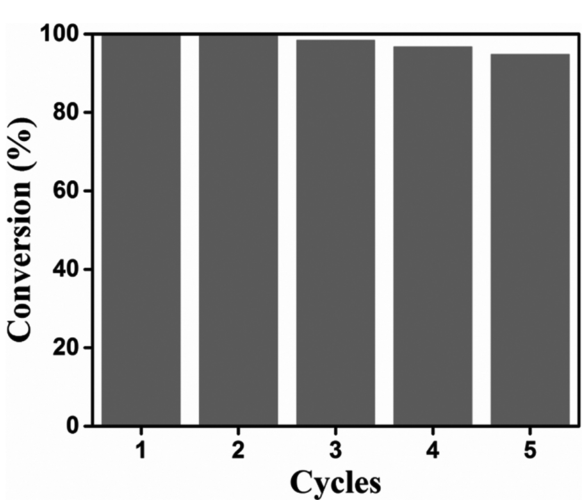

Fig. 9. Cycle tests of Cu/Co@NCF-15 for the reduction of 4-NP.

4. Conclusion

In summary, a novel Cu NPs and Co NPs doped N-containing composite material has been prepared by employing CuO-encapsulated ZIF-67 which was fabricated in a bottle-around-the-ship method as precursor and sacrificial template. Owing to the high specific surface area and porous structure of ZIF-67, Cu NPs can be uniformly distributed in the support material at high temperatures during pyrolysis thus retaining great catalytic activity. Anchoring Cu NPs into catalytically active support material-NCF, the composite exhibits splendid catalytic activity toward 4-NP over a number of noble-metal catalysts. Besides, the catalyst also reveals superior reusability after five cycles. We conclude that the catalyst we prepared has three advantages: (1) substituting copper and cobalt for noble metals will greatly reduce the cost; (2) Cu NPs and Co NPs can evenly discrete in NCF which are generated from the organic links of CuO@ZIF-67, and NCF can not only serves as supported material but also catalyst toward 4-NP, thereby enhancing the reduction activity of this catalyst; (3) the introduction of copper can elevate the content of N, which can boost the catalytic ability of the

prepared catalyst. Based on the advantages of Cu/Co@NCF, we consider that the novel composite with cost effectiveness, great catalytic activity and superior reusability can be used as a substitute for noble-metal catalysts in industrialization.

Acknowledgements

This research was financed by grants from the National Natural Science Foundation of China (21673143), Natural Science Foundation of Beijing Municipality (2172016), and Capacity Building for Sci-Tech Innovation-Fundamental Scientific Research Funds (19530050179).

Appendix A. Supplementary data

Supplementary material related to this article can be found, in the online version, at doi:https://doi.org/10.1016/j.apcatb.2019.117792.

References

[1] C.M. Malengreaux, S.L. Pirard, J.R. Bartlett, B. Heinrichs, Kinetic study of 4-nitrophenol photocatalytic degradation over a Zn^{2+} doped TiO_2 catalyst prepared through an environmentally friendly aqueous sol-gel process, Chem. Eng. J. 245 (2014) 180–190.
[2] N. Takahashi, T. Nakai, Y. Satoh, Y. Katoh, Variation of biodegradability of nitrogenous organic compounds by ozonation, Water Res. 28 (1994) 1563–1570.
[3] J. Kiwi, C. Pulgarin, P. Peringer, Effect of Fenton and photo-Fenton reactions on the degradation and biodegradability of 2 and 4-nitrophenols in water treatment, Appl. Catal. B Environ. 3 (1994) 335–350.
[4] M.A. Oturan, J. Peiroten, P. Chartrin, A.J. Acher, Complete destruction of p-nitrophenol in aqueous medium by electro-Fenton method, Environ. Sci. Technol. 34 (2000) 3474–3479.
[5] Z. Hasan, D.-W. Cho, C.-M. Chon, K. Yoon, H. Song, Reduction of p-nitrophenol by magnetic Co-carbon composites derived from metal organic frameworks, Chem. Eng. J. 298 (2016) 183–190.
[6] W. Zhang, X. Xiao, T. An, Z. Song, J. Fu, G. Sheng, M. Cui, Kinetics, degradation pathway and reaction mechanism of advanced oxidation of 4-nitrophenol in water by a UV/H_2O_2 process, J. Chem. Technol. Biotechnol. 78 (2003) 788–794.
[7] S. Liu, J. Wang, W. Huang, X. Tan, H. Dong, B.A. Goodman, H. Du, F. Lei, K. Diao, Adsorption of phenolic compounds from water by a novel ethylenediamine rosin-based resin: interaction models and adsorption mechanisms, Chemosphere 214 (2019) 821–829.
[8] Q.-S. Liu, T. Zheng, P. Wang, J.-P. Jiang, N. Li, Adsorption isotherm, kinetic and mechanism studies of some substituted phenols on activated carbon fibers, Chem. Eng. J. 157 (2010) 348–356.
[9] G. Zhang, Y. Gao, Y. Zhang, Y. Guo, Fe_2O_3-pillared rectorite as an efficient and stable fenton-like heterogeneous catalyst for photodegradation of organic contaminants, Environ. Sci. Technol. 44 (2010) 6384–6389.
[10] W.-Y. Ahn, S.A. Sheeley, T. Rajh, D.M. Cropek, Photocatalytic reduction of 4-nitrophenol with arginine-modified titanium dioxide nanoparticles, Appl. Catal. B Environ. 74 (2007) 103–110.
[11] S. Gazi, A. Rajakumar, Metal-free-photocatalytic reduction of 4-nitrophenol by resin-supported dye under the visible irradiation, Appl. Catal. B Environ. 105 (2011) 317–325.
[12] C. Wang, R. Ciganda, L. Salmon, D. Gregurec, J. Irigoyen, S. Moya, J. Ruiz, D. Astruc, Highly efficient transition metal nanoparticle catalysts in aqueous solutions, Angew. Chem. Int. Ed. 55 (2016) 3091–3095.
[13] R. Liu, S.M. Mahurin, C. Li, R.R. Unocic, J.C. Idrobo, H. Gao, S.J. Pennycook, S. Dai, Dopamine as a carbon source: the controlled synthesis of hollow carbon spheres and yolk-structured carbon nanocomposites, Angew. Chem. Int. Ed. 50 (2011) 6799–6802.
[14] M. Martin-Martinez, M.F.F. Barreiro, A.M.T. Silva, J.L. Figueiredo, J.L. Faria, H.T. Gomes, Lignin-based activated carbons as metal-free catalysts for the oxidative degradation of 4-nitrophenol in aqueous solution, Appl. Catal. B Environ. 219 (2017) 372–378.
[15] J. Li, C. Liu, Y. Liu, Au/graphene hydrogel: synthesis, characterization and its use for catalytic reduction of 4-nitrophenol, J. Mater. Chem. 22 (2012) 8426–8430.
[16] K. Tedsree, T. Li, S. Jones, C.W. Chan, K.M. Yu, P.A. Bagot, E.A. Marquis, G.D. Smith, S.C. Tsang, Hydrogen production from formic acid decomposition at room temperature using a Ag-Pd core-shell nanocatalyst, Nat. Nanotechnol. 6 (2011) 302–307.
[17] Y. Wang, L. Li, W. Yao, S. Song, J.T. Sun, J. Pan, X. Ren, C. Li, E. Okunishi, Y.Q. Wang, E. Wang, Y. Shao, Y.Y. Zhang, H.T. Yang, E.F. Schwier, H. Iwasawa, K. Shimada, M. Taniguchi, Z. Cheng, S. Zhou, S. Du, S.J. Pennycook, S.T. Pantelides, H.J. Gao, Monolayer $PtSe_2$, a new semiconducting transition-metal-dichalcogenide, epitaxially grown by direct selenization of Pt, Nano Lett. 15 (2015) 4013–4018.
[18] Y.-G. Guo, J.-S. Hu, L.-J. Wan, Nanostructured materials for electrochemical energy conversion and storage devices, Adv. Mater. 20 (2008) 2878–2887.
[19] Y. Zheng, Z. Ma, Dual-reaction triggered sensitivity amplification for ultrasensitive peptide-cleavage based electrochemical detection of matrix metalloproteinase-7, Biosens. Bioelectron. 108 (2018) 46–52.
[20] N. Liu, X. Chen, Z. Ma, Ionic liquid functionalized graphene/Au nanocomposites and its application for electrochemical immunosensor, Biosens. Bioelectron. 48 (2013) 33–38.
[21] T. Zeng, X. Zhang, S. Wang, Y. Ma, H. Niu, Y. Cai, A double-shelled yolk-like structure as an ideal magnetic support of tiny gold nanoparticles for nitrophenol reduction, J. Mater. Chem. A 1 (2013) 11641–11647.
[22] J. Shen, Y. Zhou, J. Huang, Y. Zhu, J. Zhu, X. Yang, W. Chen, Y. Yao, S. Qian, H. Jiang, C. Li, In-situ SERS monitoring of reaction catalyzed by multifunctional Fe_3O_4@TiO_2@Ag-Au microspheres, Appl. Catal. B Environ. 205 (2017) 11–18.
[23] Z. Yan, L. Fu, X. Zuo, H. Yang, Green assembly of stable and uniform silver nanoparticles on 2D silica nanosheets for catalytic reduction of 4-nitrophenol, Appl. Catal. B Environ. 226 (2018) 23–30.
[24] J. Zhang, G. Chen, D. Guay, M. Chaker, D. Ma, Highly active PtAu alloy nanoparticle catalysts for the reduction of 4-nitrophenol, Nanoscale 6 (2014) 2125–2130.
[25] Q. Wang, J. Wang, D. Wang, M. Turhong, M. Zhang, Recyclable and effective Pd/poly(N-isopropylacrylamide) catalyst for hydrodechlorination of 4-chlorophenol in aqueous solution, Chem. Eng. J. 280 (2015) 158–164.
[26] X. Yang, H. Zhong, Y. Zhu, H. Jiang, Shen J, J. Huang, C. Li, Highly efficient reusable catalyst based on silicon nanowire arrays decorated with copper nanoparticles, J. Mater. Chem. A 2 (2014) 9040–9047.
[27] W.-J. Liu, K. Tian, H. Jiang, H.-Q. Yu, Harvest of Cu NP anchored magnetic carbon materials from Fe/Cu preloaded biomass: their pyrolysis, characterization, and catalytic activity on aqueous reduction of 4-nitrophenol, Green Chem. 16 (2014) 4198.
[28] H. Niu, S. Liu, Y. Cai, F. Wu, X. Zhao, MOF derived porous carbon supported Cu/Cu_2O composite as high performance non-noble catalyst, Microporous Mesoporous Mater. 219 (2016) 48–53.
[29] Y. Deng, Y. Cai, Z. Sun, J. Liu, C. Liu, J. Wei, W. Li, C. Liu, Y. Wang, D. Zhao, Multifunctional mesoporous composite microspheres with well-designed nanostructure: a highly integrated catalyst system, J. Am. Chem. Soc. 132 (2010) 8466–8473.
[30] S. Tang, S. Vongehr, Z. Zheng, H. Liu, X. Meng, Silver doping mediated route to bimetallically doped carbon spheres with controllable nanoparticle distributions, J. Phys. Chem. C 114 (2010) 18338–18346.
[31] L. Ai, H. Yue, J. Jiang, Environmentally friendly light-driven synthesis of Ag nanoparticles in situ grown on magnetically separable biohydrogels as highly active and recyclable catalysts for 4-nitrophenol reduction, J. Mater. Chem. 22 (2012) 23447.
[32] J. Yang, F. Zhang, H. Lu, X. Hong, H. Jiang, Y. Wu, Y. Li, Hollow Zn/Co ZIF particles derived from core-shell ZIF-67@ZIF-8 as selective catalyst for the semi-hydrogenation of acetylene, Angew. Chem. Int. Ed. 54 (2015) 10889–10893.
[33] G. Zhong, D. Liu, J. Zhang, The application of ZIF-67 and its derivatives: adsorption, separation, electrochemistry and catalysts, J. Mater. Chem. A 6 (2018) 1887–1899.
[34] T.D. Bennett, J.C. Tan, S.A. Moggach, R. Galvelis, C. Mellot-Draznieks, B.A. Reisner, A. Thirumurugan, D.R. Allan, A.K. Cheetham, Mechanical properties of dense zeolitic imidazolate frameworks (ZIFs): a high-pressure X-ray diffraction, nanoindentation and computational study of the zinc framework $Zn(Im)_2$, and its lithium-boron analogue, $LiB(Im)_4$, Chem. Eur. J. 16 (2010) 10684–10690.
[35] Z.-S. Hong, Y. Cao, J.-F. Deng, A convenient alcohothermal approach for low temperature synthesis of CuO nanoparticles, Mater. Lett. 52 (2002) 34–38.
[36] A.K. Patra, A. Dutta, A. Bhaumik, Cu nanorods and nanospheres and their excellent catalytic activity in chemoselective reduction of nitrobenzenes, Catal. Commun. 11 (2010) 651–655.
[37] L. Li, T. Tian, J. Jiang, L. Ai, Hierarchically porous Co_3O_4 architectures with honeycomb-like structures for efficient oxygen generation from electrochemical water splitting, J. Power Sources 294 (2015) 103–111.
[38] M. Kuang, Q. Wang, P. Han, G. Zheng, Cu, Co-embedded N-enriched mesoporous carbon for efficient oxygen reduction and hydrogen evolution reactions, Adv. Energy Mater. 7 (2017) 1700193.
[39] A. Zhou, R.-M. Guo, J. Zhou, Y. Dou, Y. Chen, J.-R. Li, Pd@ZIF-67 derived recyclable Pd-based catalysts with hierarchical pores for high-performance heck reaction, ACS Sustain. Chem. Eng. 6 (2018) 2103–2111.
[40] N.L. Torad, M. Hu, S. Ishihara, H. Sukegawa, A.A. Belik, M. Imura, K. Ariga, Y. Sakka, Y. Yamauchi, Direct synthesis of MOF-derived nanoporous carbon with magnetic Co nanoparticles toward efficient water treatment, Small 10 (2014) 2096–2107.
[41] X. Li, C. Zeng, J. Jiang, L. Ai, Magnetic cobalt nanoparticles embedded in hierarchically porous nitrogen-doped carbon frameworks for highly efficient and well-recyclable catalysis, J. Mater. Chem. A 4 (2016) 7476–7482.
[42] K. Shen, L. Chen, J. Long, W. Zhong, Y. Li, MOFs-templated Co@Pd core-shell NPs embedded in N-doped carbon matrix with superior hydrogenation activities, ACS Catal. 5 (2015) 5264–5271.
[43] Z. Hasan, Y.S. Ok, J. Rinklebe, Y.F. Tsang, D.-W. Cho, H. Song, N doped cobalt-carbon composite for reduction of p-nitrophenol and pendimethaline, J. Alloys Compd. 703 (2017) 118–124.
[44] H. Wu, H. Li, X. Zhao, Q. Liu, J. Wang, J. Xiao, S. Xie, R. Si, F. Yang, S. Miao, X. Guo, G. Wang, X. Bao, Highly doped and exposed Cu(I)-N active sites within graphene towards efficient oxygen reduction for zinc-air batteries, Energy Environ. Sci. 9 (2016) 3736–3745.
[45] B. Volosskiy, H. Fei, Z. Zhao, S. Lee, M. Li, Z. Lin, B. Papandrea, C. Wang, Y. Huang, X. Duan, Tuning the catalytic activity of a metal-organic framework derived copper and nitrogen Co-doped carbon composite for oxygen reduction reaction, ACS Appl. Mater. Inter. 8 (2016) 26769–26774.
[46] Z. Zhang, M. Dou, H. Liu, L. Dai, F. Wang, A facile route to bimetal and nitrogen-codoped 3D porous graphitic carbon networks for efficient oxygen reduction, Small

12 (2016) 4193–4199.
[47] Y. Qian, Z. Liu, H. Zhang, P. Wu, C. Cai, Active site structures in nitrogen-doped carbon-supported cobalt catalysts for the oxygen reduction reaction, ACS Appl. Mater. Interface 8 (2016) 32875–32886.
[48] J. Wei, Y. Liang, Y. Hu, B. Kong, J. Zhang, Q. Gu, Y. Tong, X. Wang, S.P. Jiang, H. Wang, Hydrothermal synthesis of metal-polyphenol coordination crystals and their derived metal/N-doped carbon composites for oxygen electrocatalysis, Angew. Chem. Int. Ed. 55 (2016) 12470–12474.
[49] A.K. Sasmal, S. Dutta, T. Pal, A ternary Cu2O-Cu-CuO nanocomposite: a catalyst with intriguing activity, Dalton Trans. 45 (2016) 3139–3150.
[50] A. Saha, B. Ranu, Highly chemoselective reduction of aromatic nitro compounds by copper nanoparticles/ammonium formate, J. Org. Chem. 73 (2008) 6867–6870.
[51] N. Pradhan, A. Pal, T. Pal, Catalytic reduction of aromatic nitro compounds by coinage metal nanoparticles, Langmuir 17 (2001) 1800–1802.
[52] P. Zhang, C. Shao, Z. Zhang, M. Zhang, J. Mu, Z. Guo, Y. Liu, In situ assembly of well-dispersed Ag nanoparticles (AgNPs) on electrospun carbon nanofibers (CNFs) for catalytic reduction of 4-nitrophenol, Nanoscale 3 (2011) 3357–3363.
[53] K. Layek, M.L. Kantam, M. Shirai, D. Nishio-Hamane, T. Sasaki, H. Maheswaran, Gold nanoparticles stabilized on nanocrystalline magnesium oxide as an active catalyst for reduction of nitroarenes in aqueous medium at room temperature, Green Chem. 14 (2012) 3164.